Australian Journal of Mechanical Engineering

ISSN: (Print) (Online) Journal homepage: https://engineersaustralia.tandfonline.com/loi/tmec20

A comparative analysis of thermo-hydraulic performance of a roughened solar air heater using various rib shapes

Vipin B. Gawande , A. S. Dhoble , D. B. Zodpe & Chidanand Mangrulkar

To cite this article: Vipin B. Gawande , A. S. Dhoble , D. B. Zodpe & Chidanand Mangrulkar (2020) A comparative analysis of thermo-hydraulic performance of a roughened solar air heater using various rib shapes, Australian Journal of Mechanical Engineering, 18:3, 331-350, DOI: 10.1080/14484846.2018.1525171

To link to this article: https://doi.org/10.1080/14484846.2018.1525171

Published online: 08 Oct 2018.

AUSTRALIAN JOURNAL OF MECHANICAL ENGINEERING
2020, VOL. 18, NO. 3, 331–350
https://doi.org/10.1080/14484846.2018.1525171

Taylor & Francis
Taylor & Francis Group

ARTICLE

A comparative analysis of thermo-hydraulic performance of a roughened solar air heater using various rib shapes

Vipin B. Gawande[a], A. S. Dhoble[b], D. B. Zodpe[b] and Chidanand Mangrulkar[b]

[a]Department of Mechanical Engineering, Vidya Pratishthan's Kamalnayan Bajaj Institute of Engineering and Technology, Baramati, India; [b]Department of Mechanical Engineering, Visvesvaraya National Institute of Technology, Nagpur, India

ABSTRACT

The thermal efficiency of the solar air heater (S.A.H.) is enhanced by introducing various artificial roughness geometries on the absorber surface. Artificial roughnesses in the form of a chamfered rib, right angle triangular and reverse L-shaped ribs, invented from square rib are presented. A comparative thermohydraulic analysis of these ribs is carried out using experimental, Computational Fluid Dynamics (C.F.D.) and analytical investigation. The experiments are carried out using rib height (e = 0.7,1 and 1.4), relative roughness pitch (P/e = 7.14 to 35.71), relative roughness height (e/D = 0.021, 0.03 and 0.042), Reynolds number (Re = 3800 to 18000) and duct aspect ratio (W/H= 5).The effect of rib shape, rib height (e), pitch (P), relative roughness pitch (P/e), relative roughness height (e/D), chamfer angle (α) and Reynolds number (Re) on heat transfer and friction flow is evaluated. Experimental results are validated using C.F.D. code ANSYS FLUENT 14.5, by simulating two-dimensional computational domain of roughened S.A.H. Based on the experimental results correlations for the Nusselt number and friction factor are derived. A mathematical model has been developed to investigate the effect of geometrical and operating parameters on the thermal and effective efficiency of a roughened S.A.H.

ARTICLE HISTORY
Received 16 February 2018
Accepted 13 September 2018

KEYWORDS
Computational Fluid Dynamics; solar air heater; solar energy; artificial roughness; thermo-hydraulic performance parameter; friction factor

1. Introduction

Solar air heaters (S.A.H.s) form the foremost component of solar energy utilisation system. These air heaters absorb the irradiance and convert it into thermal energy at the absorbing surface and then transfer the energy to a fluid flowing through the collector. S.A.H.s are inexpensive and the most used collection devices because of their inherent simplicity. S.A.H.s are generally considered to be useful for applications including space heating, crop drying, seasoning of timber, curing of industrial products and curing/drying of concrete/clay building components. The thermal performance of a S.A.H. is significantly low because of the low value of the convective heat transfer coefficient between the absorber plate and the air, leading to high absorber plate temperature and greater heat losses the surroundings. It has been found that the main thermal resistance to the heat transfer is due to the formation of a laminar sub-layer on the heat-transferring surface. Efforts of improving the heat transfer rate have been directed towards artificially sub-layer. An artificial roughness on the heat transfer surface in the form of projections mainly creates turbulence near the wall, breaks the laminar sub-layer and, thus, enhances the heat transfer coefficient with a minimum pressure loss penalty. Artificial roughness in various geometrical shapes has been employed for the enhancement of the heat transfer coefficient. However, this also brings about a substantial increase in pumping power. To evaluate thermal, hydraulic and thermo-hydraulic performance, S.A.H. was analysed using experimental, theoretical or analytical and numerical or computational approach (i.e. C.F.D.) in the literature.

The physics of fluid and heat flow in a S.A.H. is expressed in the form of mathematical equations (differential or integral) and is solved using analytical/mathematical approach. In the literature, Ong (1995) has developed a mathematical model and procedure for predicting thermal performance of single-pass solar air collectors. Bhushan and Singh (2012) have evaluated thermal and thermo-hydraulic performance of roughened S.A.H. having protruded absorber plate using a mathematical model. An analytical approach was used by Ammari (2003) to develop a mathematical model for predicting thermal performance of a S.A.H. with slats. An exact analytical solution for fully developed convective heat transfer in rectangular ducts under a constant heat flux was derived by Shamardan et al. (2012). A detailed explanation of various roughness geometries used by researchers in past for their experimental investigations is given in author's review paper written on roughness geometries in S.A.H.s (Gawande, Dhoble, and Zodpe 2014). The correlations developed for heat transfer and friction factor for S.A.H. having artificial roughness are tabulated in the same paper. Many

CONTACT Vipin B. Gawande vipingawande@gmail.com

researchers have investigated that results obtained from the C.F.D. analysis are in good agreement with the previous experimental results and, hence, this tool can be used to simulate S.A.H. with the various ranges of operating and geometrical parameters. A detailed review of C.F.D. methodology, used by researchers for investigating thermal performance of roughened S.A.H., is presented in author's second review paper (Gawande et al. 2016d). In the recent years, Gupta and Varshney (2017), Kumar, Goel, and Kumar (2018), Kumar et al. (2018), Kumar and Kumar (2017), Ravi and Saini (2018), Singh and Singh (2018) have contributed in the experimental and computational analysis of a roughened S.A.H. A comprehensive literature review helps to determine the research gap for present research work. Three types of ribs shape viz. chamfered, right-angle triangular and reverse L-shaped rib are carved as artificial roughness for the comparative analysis of a roughened S.A.H. Finally, the objectives for conducting present research work are derived.

- To inspect the effect of operating parameters such as relative roughness pitch (P/e), relative roughness height (e/D) and Reynolds number (Re) on the enhancement of Nusselt number and friction characteristics of an artificially roughened S.A.H.
- To develop correlations for heat transfer coefficient (Nusselt number) and friction factor in terms of flow and geometrical parameters for newly carved ribs
- To develop an analytical model for predicting the thermal performance of roughened S.A.H. with chamfered, right-angle triangular and reverse L-shaped ribs
- To compare the thermal performance of three types of ribbed duct. Thermal performance of roughened duct is compared with previously investigated ribs in literature and smooth duct.

2. Experimental and C.F.D. approach

The wooden rectangular duct has internal size as 640 mm × 100 mm × 20 mm, with an aspect ratio (W/H) of 5. The test section has a length of 280 mm with a cross section of 100 mm × 20 mm. It consists of an entrance section, a test section and an exit section having lengths as 245, 280 and 115 mm, respectively. For the turbulent flow regime, ASHRAE Standard (1977) recommends entry and exit lengths as $5\sqrt{W \times H}$ and 2.5 $\sqrt{W \times H}$, respectively; this has been used in designing the duct for this experimental work. The test section consists of G.I plates of 3 mm thicknesses, which is roughened at the wetted side by angled (chamfered) rib, right-angle triangular rib and reverse L-shaped rib using superglue adhesive, and all other three wooden sides are smooth. An electric heating element was fabricated by combining five loops of nichrome wire in series and parallel, having a size of 280 mm × 100 mm, to supply a uniform heat flux of 1000 W/m^2 to the absorber plate, which is considered to be reasonably having a good value of heat energy input for testing S.A.H.s. It has been observed that creating artificial roughness on the absorber plate is a tedious task and carving ribs of required shape on the absorber plate demands skilful workmanship. So, the ribs are created using 3-D printing machine with white acrylonitrile butadiene styrene (ABS) material. Air drawn at room temperature is sucked through the duct by means of a centrifugal blower. For precise control of the air flow rate through the system, gate valve is provided, on the outlet side of the blower. The rate of air flow through the duct is measured by a flange type orifice metre. The K-type copper constantan calibrated thermocouples are used to record the plate temperature in test section, inlet and outlet temperatures. All the thermocouples are connected to the digital temperature measurement devices for measuring temperatures. The pressure drop across the test section of the duct was measured with the help of a micro-manometer. A schematic and pictorial of experimental set up used for the present work is shown in Figures 1 and 2.

The chamfered, right-angle triangular and reverse L-shaped ribs are shown in Figure 3. The effect of rib shape of three roughness geometries modified from the square rib has been used under the present investigation. The cross section of roughness is described by the values of rib height (e) and rib pitch (P). The range of parameters for this study has been decided on the basis of

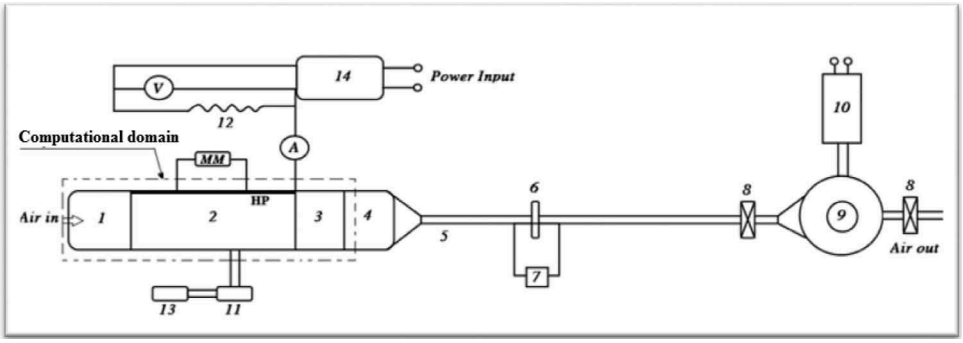

Figure 1. Schematic of experimental set up.

Figure 2. Pictorial view of experimental set up (Gawande et al. 2016c).

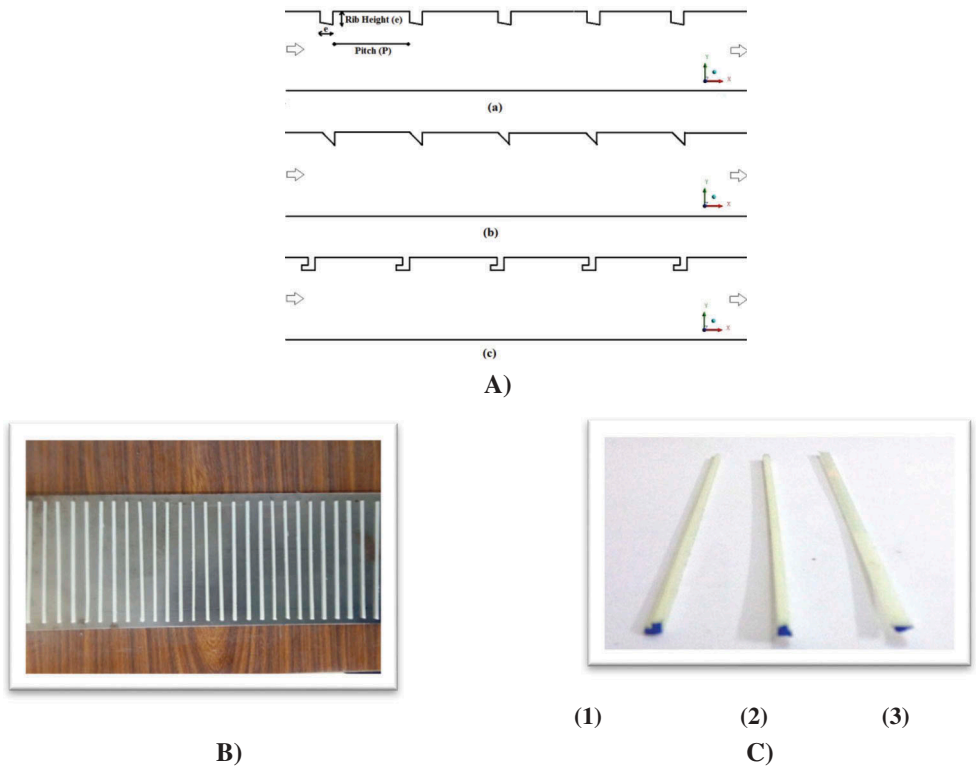

Figure 3. Roughness geometries used in the analysis (Gawande et al. 2016a, 2016b, 2016c).

Table 1. Range of operating parameters used in artificially roughened S.A.H. duct.

Operating parameters	Range
Uniform heat flux (q)	1000 W/m^2
Reynolds Number (Re)	3800–18,000 (6 values)
Relative roughness pitch (P/e)	7.14 – 35.71 (12 values)
Relative roughness height (e/D)	0.021–0.042 (3 values)
Chamfer angle (α)	0°–40°

practical considerations of the system and operating conditions of the S.A.H. and is given in Table 1. The minimum rib height is chosen such that the laminar sub-layer would be of same order as roughness height at the lower flow Reynolds number. The maximum rib height is 1.4 mm so that the flow passage blockage effects are negligible. Table 2 shows different configurations of angled (chamfered) rib, right-angle triangular rib and reverse L-shaped rib roughness used in experimental and C.F.D. investigation. Total 36 configurations using these three types of ribs are

Table 2. Different configurations of angled (chamfered) rib, right-angle triangular rib and reverse L-shaped rib roughness used in experimental and C.F.D. investigation.

Roughness Configuration	Hydraulic diameter of duct, D (mm)	Rib height, e (mm)	Relative roughness height, e/D	Rib pitch, P (mm)	Relative roughness pitch, P/e
Type-1	33.33	0.7	0.021	10	14.29
Type-2				15	21.43
Type-3				20	28.57
Type-4				25	35.71
Type-5	33.33	1	0.03	10	10
Type-6				15	15
Type-7				20	20
Type-8				25	25
Type-9	33.33	1.4	0.042	10	7.14
Type-10				15	10.71
Type-11				20	14.29
Type-12				25	17.86

investigated experimentally and using C.F.D. tool. Data under similar operating conditions have been collected for smooth duct for the purpose of validation.

C.F.D. technique is used to solve the flow physics for the predefined boundary condition. C.F.D. helps the researchers to predict the performance of the given system before its actual installation. C.F.D. simulates the real system; work out the flow equations using mathematical techniques and various current models. It has been observed that the results predicted by C.F.D. are in good agreement with the actual experimental results. The modelling of the S.A.H. duct is carried out using design modeller of ANSYS 14.5.

To analyse the fluid flow in the computational domains (as shown in Figure 4), flow domains are split into smaller sub-domains called cells and discretised governing equations are solved inside each cell. The complete solution of the fluid flow is the compilation of the results in each cell. In this work, two-dimensional non-uniform grid is generated in the computational domain, in the meshing module of ANSYS 14.5 as shown in Figure 5. Mesh sensitivity analysis has been carried out to for all ribs, to check the influence of mesh quality on simulation results. Mesh sensitivity analysis carried out for reversed L-shaped ribs is shown in Table 3. Minor variation in results are predicted after grid size of 211528 in Nusselt number and friction factor and, hence, selected for further C.F.D. analysis.

A C.F.D. code ANSYS 14.5 is used to convert the partial differential governing equations into algebraic equations using a control volume technique. The governing equations are formulated considering the fluid flow as a single-phase, incompressible, no radiation heat transfer and fully developed flow (steady state condition).

In C.F.D. code, ANSYS F.L.U.E.N.T. 14.5, the inlet velocity magnitude calculated using the Reynolds number in the range of 1.67–7.9 m/s, percentage turbulent intensity and hydraulic diameter is specified at the inlet of computational domain of S.A.H. The temperature of the inlet air is maintained at 300 K. A constant heat flux of 1000 W/m^2 is specified on the top surface of the absorber plate in test section. The material of the absorber plate is selected as aluminium. The ribs are assumed adiabatic, initially at 300 K. At exit, outlet boundary condition is specified in the form of fixed atmospheric pressure (1.013×10^5 Pa). In the present analysis, to study the forced convection and fully developed turbulent flow in a S.A.H. duct, a RNG k-ε turbulence model is used to predict the effect of turbulence on heat transfer enhancement and friction factor characteristics. For pressure velocity coupling, S.I.M.P.L.E. (Semi Implicit Method for Pressure Linked Equations) algorithm suggested by Patankar (1980) is used during the discretisation of governing equations. Second-order upwind discretisation scheme is applied

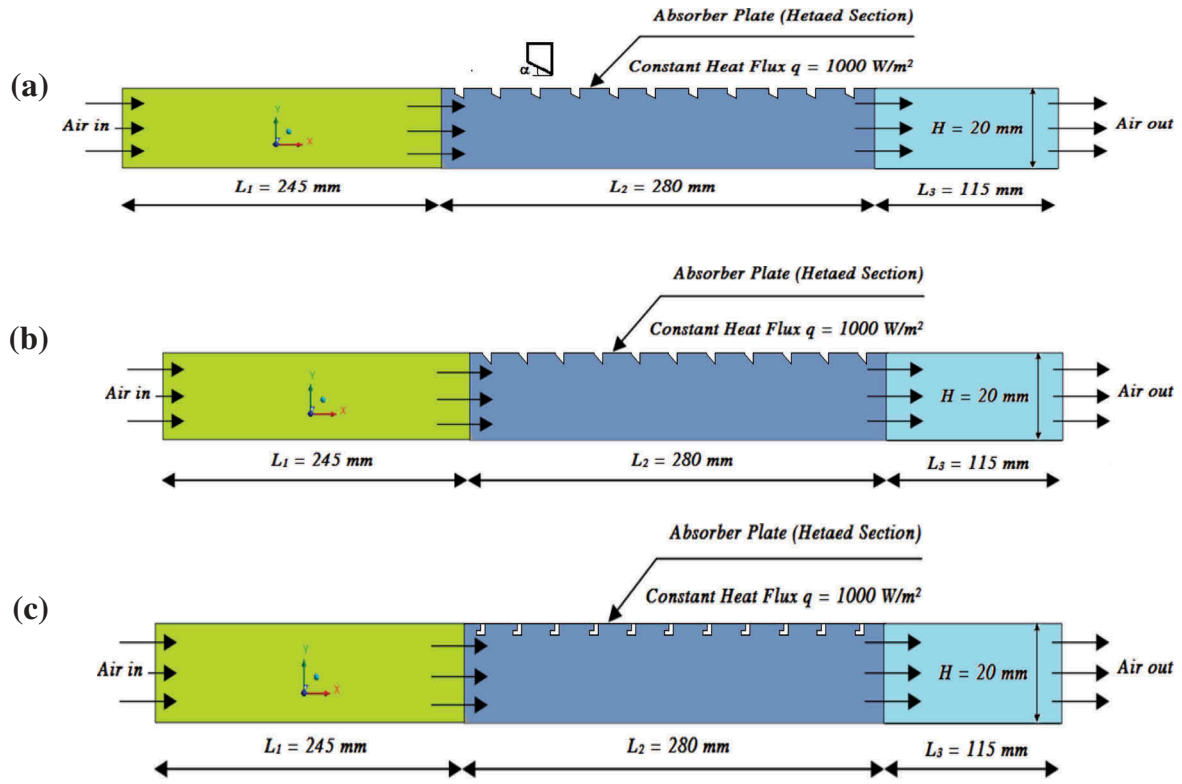

Figure 4. Schematic of two-dimensional domain of S.A.H. for (a) chamfered rib (b) right-angle triangular rib and (c) reverse L-shaped rib. (Gawande et al. 2016a, 2016b, 2016c).

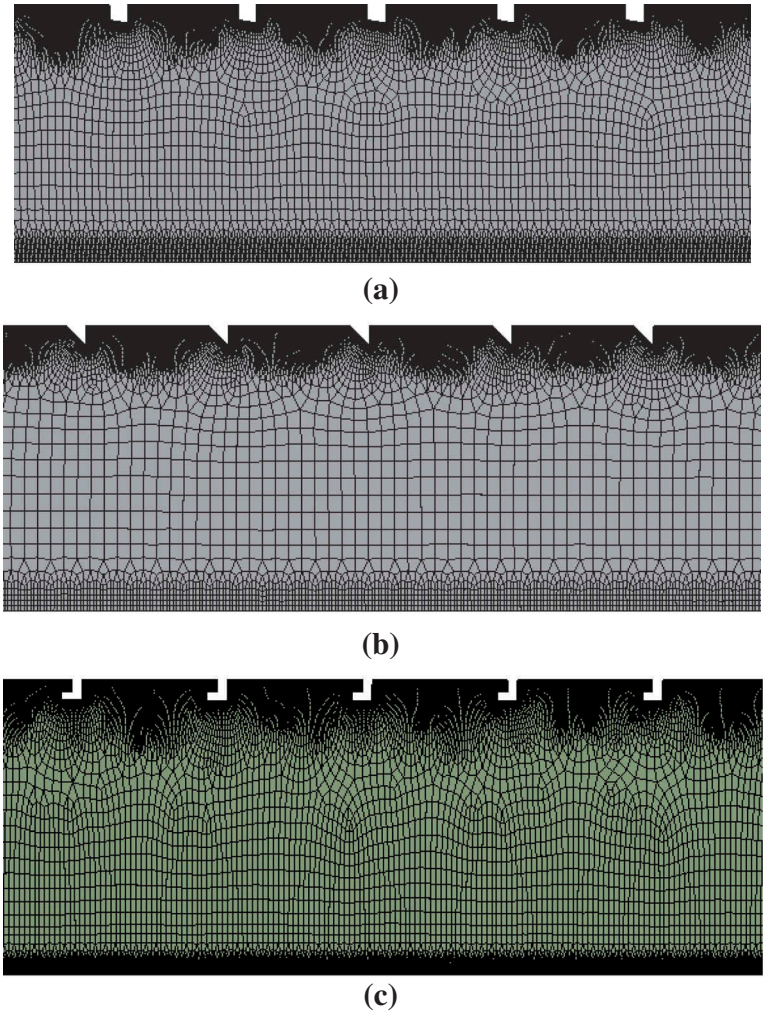

Figure 5. Two-dimensional non-uniform grid generation on computational domain for (a) chamfered rib (b) right-angle triangular rib and (c) reverse L-shaped rib. (Gawande et al. 2016a, 2016b, 2016c).

Table 3. Mesh sensitivity analysis for reversed L-shaped ribs (Gawande et al. 2016c).

Sl. No.	Number of elements	Nusselt Number (Nu)	% difference	Friction factor (f)	% difference
1	185254	149.33	-	0.0237	-
2	195269	152.28	1.95	0.0246	3.72
3	199358	153.04	0.49	0.0249	1.21
4	**211528**	**152.75**	**0.18**	**0.0250**	**0.40**
5	220154	152.95	0.13	0.0251	0.39

to all the transport equations. To achieve higher accuracy, the convergence criteria between two consecutive iterations is set to be relative deviation less than 10^{-6} for energy equation and less than 10^{-3} for solution in velocity and the continuity equation. The discretised conservation equations are solved iteratively until convergence. The results are examined to review solution and extract useful data. After examining the results, necessary revisions or modifications are made in the domain to obtain results with different operating condition. A series of test runs were conducted to generate data with individual parameters varied whilst the other parameters kept constant. The recorded data were utilised for determining heat transfer coefficient (Nusselt number) and friction factor. A MATLAB code has been developed for the analytical analysis of roughened S.A.H.

3. Results and discussion

A S.A.H. involves the physics of fluid and heat flow. The fluid and heat flow physics of a S.A.H. can be predicted using its thermal, hydraulic and thermo-hydraulic performance. Thermal performance of a S.A.H. involves evaluating heat transfer coefficient (h) and converting it into non-dimensionless Nusselt number (Nu) and thermal efficiency (η_{th}).

A thorough check of experimental set up was carried out by conducting experimentation on smooth duct for all cases. Accuracy of Nusselt number and friction factor data collected for smooth duct was verified by comparing it with the data obtained from following Nusselt number and friction factor correlations reported by Dittus-Boelter (McAdams (1942)) **and** Blassius (Fox, Pritchard, and McDonald 2010), respectively. Comparison of experimental and predicted data of Nusselt number and friction factor is shown in Figures 6 and 7, respectively. The average

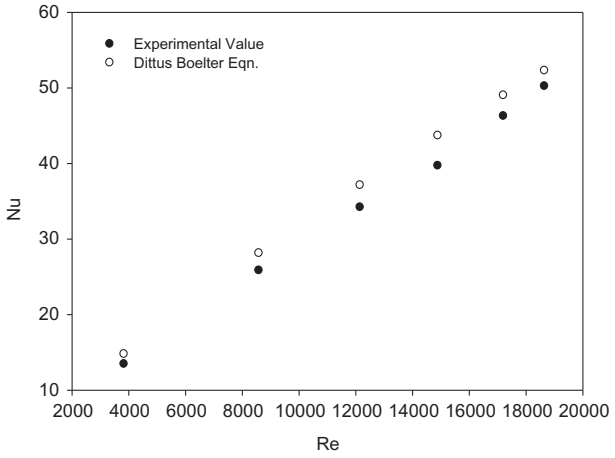

Figure 6. Comparison of experimental and predicted values from Dittus-Boelter equation of Nusselt number.

absolute deviation between the predicted and experimental values of Nusselt number and friction factor for all cases were found in the range of 1.67–2%, respectively. Hence, a reasonably good agreement between experimental and predicted data ensures accuracy of the data being collected with the help of the experimental set up. The RNG-k-ε turbulence model is selected by comparing the correlations results with the results obtained from the available turbulence models in the C.F.D. code ANSYS F.L.U.E.N.T. The comparison is shown in Figure 8.

3.1. Effect of Reynolds number

The effect of Reynolds number on average Nusselt number for different values of relative roughness pitch (P/e) at constant e/D = 0.042 is shown in Figure 9. The average Nusselt number increases with respect to smooth duct by inserting 20° chamfered rib, right-angle triangular rib and reverse L-shaped rib on the underside of absorber plate in S.A.H. duct, with increasing values of Reynolds number. The increase in Reynolds number reduces laminar sub-layer thickness. This leads to generation of local wall turbulence due to flow separation and reattachment between the ribs, which enhances heat transfer rate. Rib tips help to generate vortices and, thus, cause flow mixing, which contributes to removal of heat from the heated absorber plate. This increases the heat transfer rate as compared to smooth surface.

For 20° chamfered rib, the maximum enhancement in Nusselt number has been found to be 3.218 times over the smooth duct at Re = 15,000 corresponding to relative roughness pitch (P/e) of 7.14 for constant relative roughness height of 0.042. The minimum value of average Nusselt number is obtained at relative roughness pitch (P/e) of 17.86 for the range of parameters investigated. This value of Nusselt number has been reported as 2.339 times over the smooth duct at Re = 3800. The maximum enhancement of the Nusselt number for the right-angle triangular rib has been found to be 3.10 times that of the smooth duct for relative roughness pitch of 7.14 and relative roughness height of 0.042. In the range of parameter investigated, the maximum enhancement of average Nusselt number occurs at a Reynolds number of 15,000. The maximum enhancement in the Nusselt number for reverse L-shaped ribs is found to be 2.827 times over the smooth duct corresponding to relative roughness pitch of 7.14 at constant relative roughness height of 0.042. Figure 9 shows that the increase in Reynolds number increases turbulent intensity due to increase in the turbulent dissipation rate and turbulent kinetic energy, which increases the average Nusselt number. Figure 10 shows the comparison of turbulent kinetic energy obtained from the numerical analysis (F.L.U.E.N.T.)

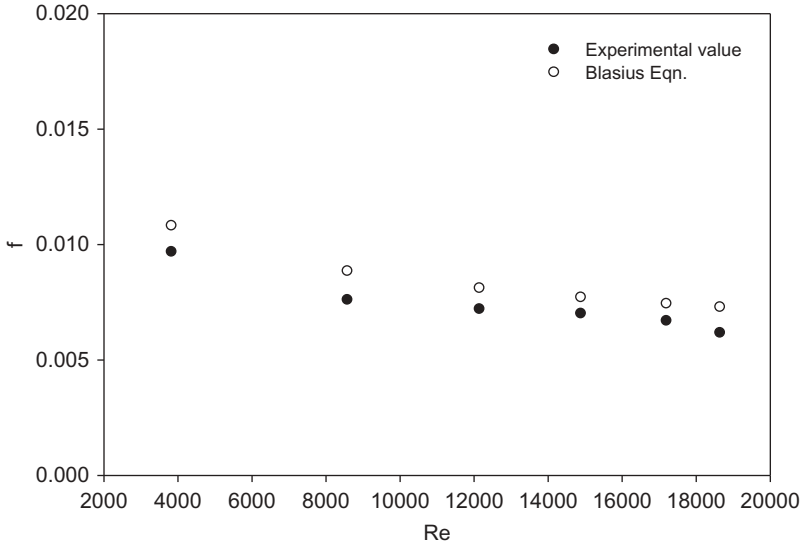

Figure 7. Comparison of experimental and predicted values from Blasius equation of friction factor.

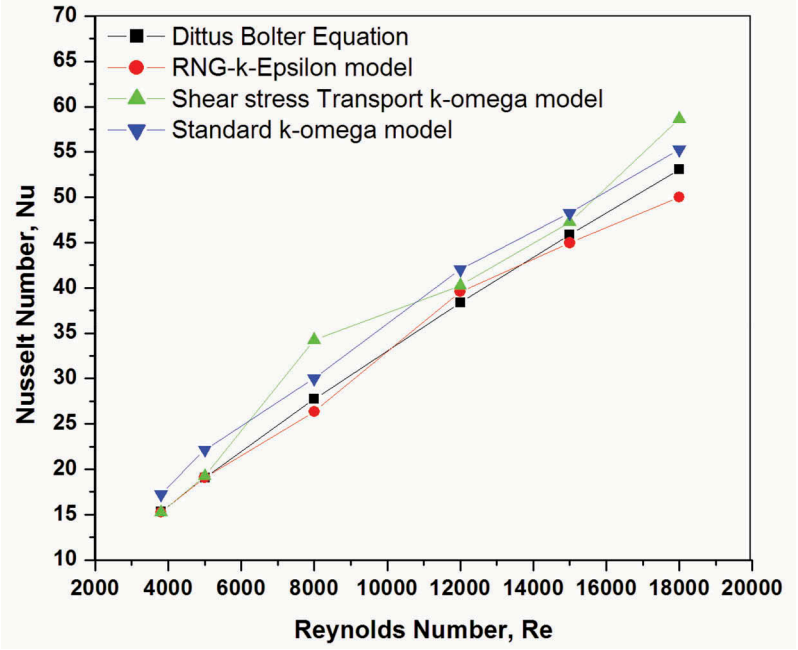

Figure 8. Comparison of average Nusselt number with various turbulence models.

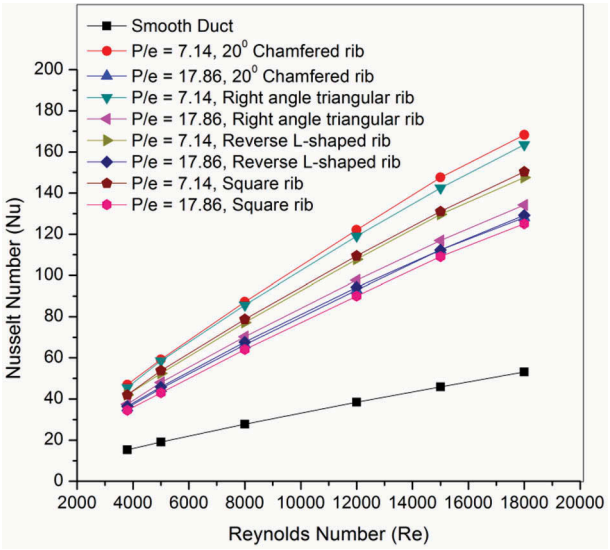

Figure 9. Variation of Nusselt number with Reynolds number for different values of *P/e* at *e/D* = 0.042. (Gawande et al. 2016a, 2016b, 2016c).

in the form of contour plots, for Reynolds number of 15,000 at the relative roughness pitch (*P/e*) of 7.14 and relative roughness height (*e/D*) of 0.042. The contour plots show that chamfered rib and right-angle triangular rib has high intensity of turbulent kinetic energy than the reverse L-shaped rib. The mean flow energy in the chamfered, right-angle triangular and reverse L-shaped rib roughened wall, which is used for convection heat transfer, is now converted into turbulent kinetic energy due to variation of Reynolds number. This shows that the chamfered, right-angle triangular and reverse L-shaped rib roughened duct has the more unremarkable effect of Reynolds number on the Nusselt number ratio than the smooth duct.

Figure 11 shows the contour plot of turbulent intensity for three ribs at Reynolds number of 15,000 and at relative roughness pitch (*P/e*) of 7.14 and relative roughness height (*e/D*) of 0.042. The increase in turbulent intensity and mixing of the flow due to generation of vortices at the rib tip causes enhancement in the Nusselt number on the roughened surface than those on the smooth surface. The maximum value of turbulent intensity is seen in the neighbourhood of the ribs due to existence of higher intensity of shear layer. It is also observed that due to insertion of roughness geometries, recirculation zone is generated, which has maximum effect near the mid plane between the ribs due to reattachment. As shown in the Figure 11, maximum turbulent intensity commonly occurred just in front of the sharp edge of the 20° chamfered rib, followed by the right-angle triangular and then reverse L-shaped rib. 20° chamfered rib and right-angle triangular rib generates more turbulent intensity, so their heat transfer performance was more enhanced than that of reverse L-shaped and square rib.

Figure 12 shows the variation of friction factor with Reynolds number for different values of relative roughness pitch (P/e) at constant value of relative roughness height (*e/D* = 0.042). The maximum enhancement of average friction factor for chamfered, right-angle triangular and reverse L-shaped roughness has been found to be 4.047, 3.800 and 3.424 times, respectively, than that of the smooth duct for relative roughness pitch of 7.14 and for relative

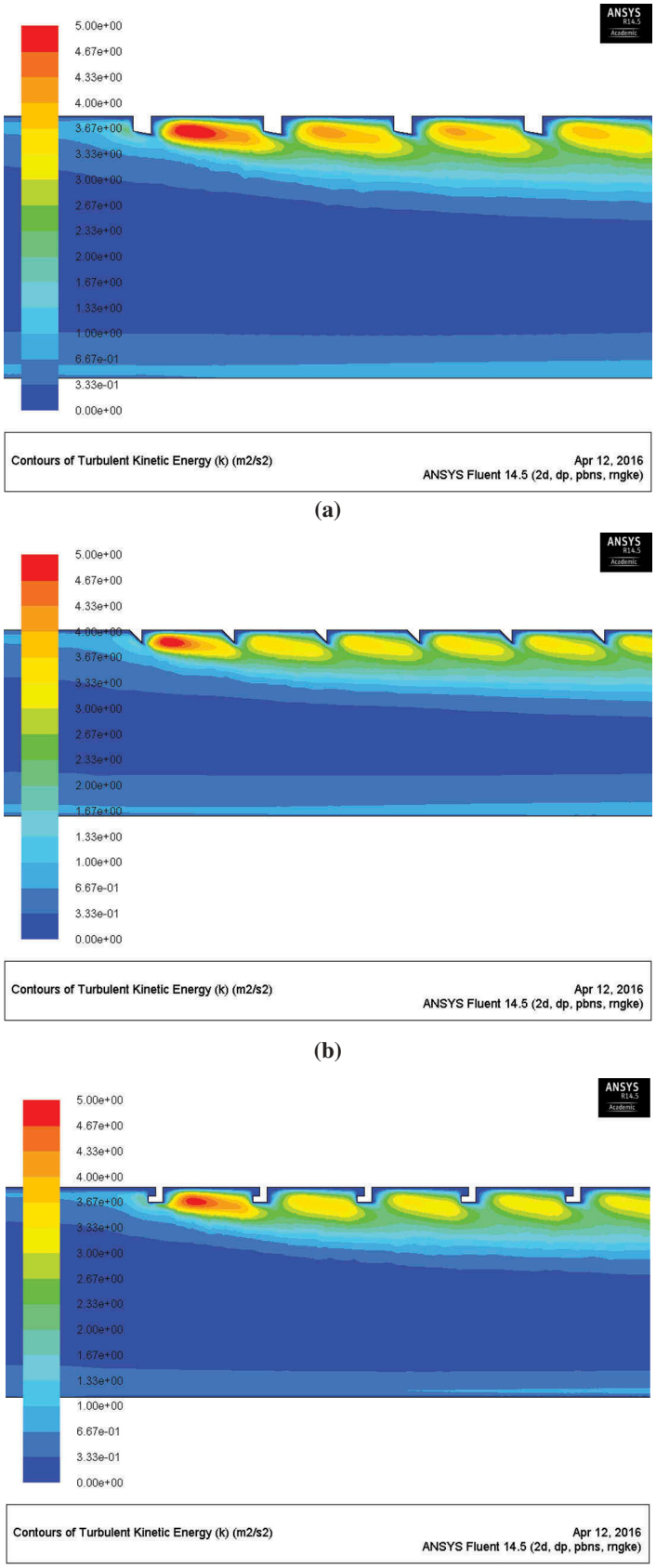

Figure 10. The contour plot of turbulent kinetic energy for P/e = 7.14 and e/D = 0.042 at a Reynolds number of 15,000 for (a) 20° chamfered, (b) right-angle triangular and (c) reverse L-shaped rib roughness. (Gawande et al. 2016a, 2016b, 2016c).

roughness height of 0.042. The maximum enhancement of average friction factor occurs at a Reynolds number of 3800 for the range of parameters investigated in the experimental study.

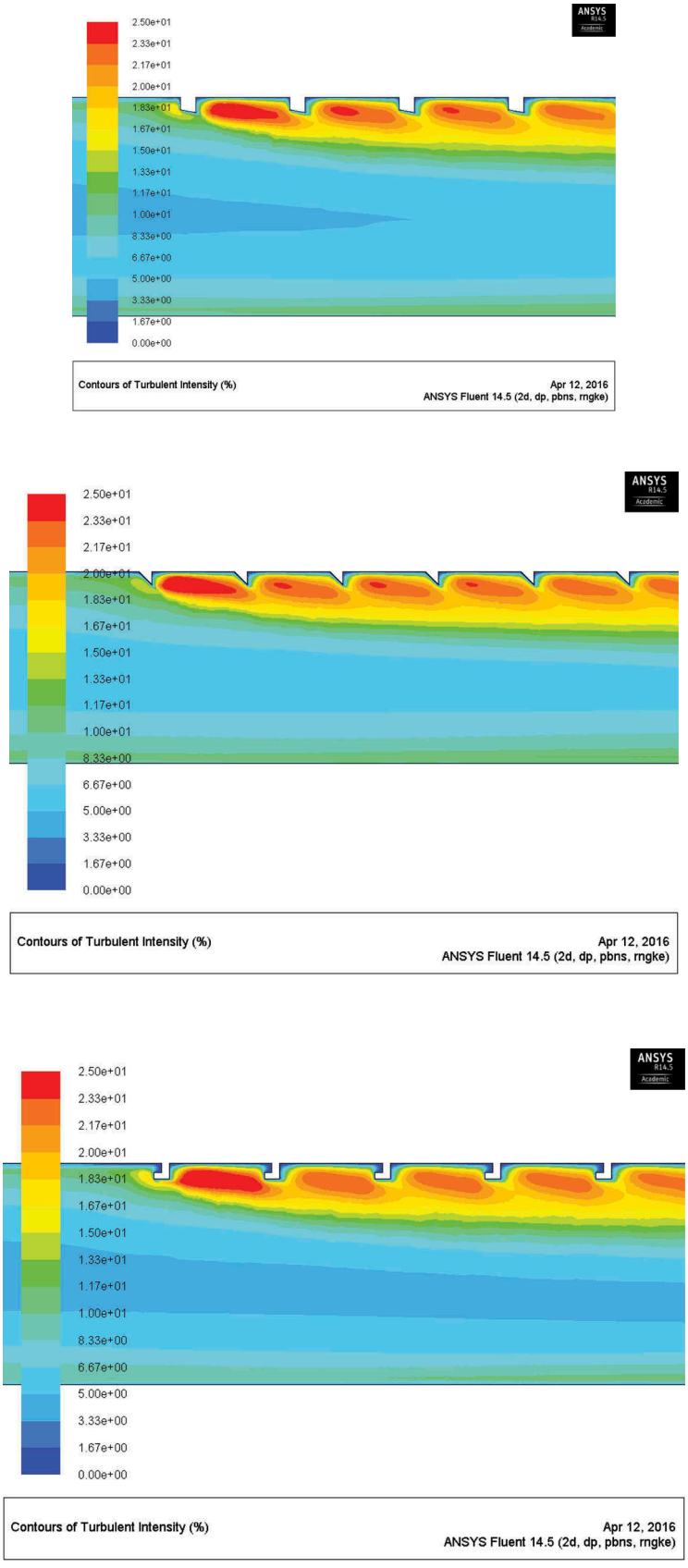

Figure 11. The contour plot of turbulent intensity for P/e = 7.14 and e/D = 0.042 at a Reynolds number of 15,000 for (a) 20° chamfered, (b) right-angle triangular and (c) reverse L-shaped rib roughness. (Gawande et al. 2016a, 2016b, 2016c).

It is observed that the friction factor decreases with increase in Reynolds number because of the suppression of viscous sub-layer. Friction factor is significantly enhanced by the presence of chamfered, right-angle triangular and reverse L-shaped ribs roughness compared to a smooth duct of a S.A.H.

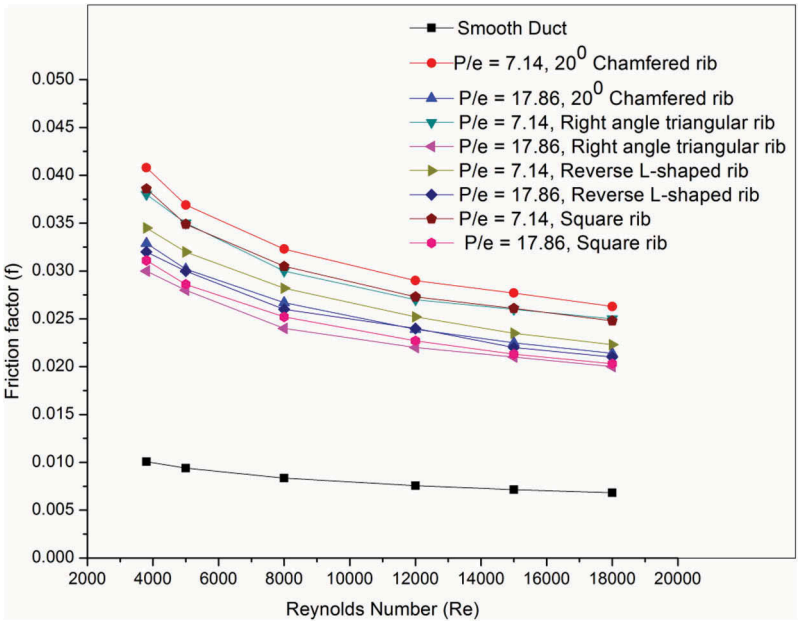

Figure 12. Variation of friction factor with Reynolds number for different values of *P/e* at *e/D* = 0.042. (Gawande et al. 2016a, 2016b, 2016c).

The flow blockage, due to presence of these ribs, is a dynamic factor to cause a high pressure drop. The hydraulic phenomenon of the artificially roughened S.A.H. having chamfered, right-angle triangular and reverse L-shaped ribs can be easily understood by examining the contour plot of pressure. A comparison plot for pressure is shown in the form of contour plots in Figure 13 for relative roughness pitch of 7.14, relative roughness height of 0.042 and Reynolds number of 15000. As the air enters the roughened region of duct of an artificially roughened S.A.H., the air starts to accelerate and results in increasing pressure drop. The pressure drop is more profound for the higher value of Reynolds number flow. In general, the resulting friction is much higher in roughened S.A.H. duct than smooth duct of a S.A.H. and it must be considered a key factor in any practical design.

Figure 14 shows the contour plots of static temperature for 20° chamfered, right-angle triangular and reverse L-shaped rib. As air passes on roughened hot surface, the heat exchange takes place from the hot surface to air. The air very close to surface gets heated due to convection. This primary hot layer mixes with the secondary cold air due to roughness, and heat transfer takes place due to conduction and convection. As a result, the temperature of air close to surface is higher, and goes on decreasing away from the surface. The turbulence generated due to presence of roughness brings cold fluid to the region near the leading end of ribs, lowers the wall temperature and, hence, increases the local heat transfer coefficient. For roughened S.A.H. duct the maximum Nusselt number is more for 20° chamfered ribs followed by right-angle triangular rib and then reverse L-shaped rib for the range of Reynolds number investigated.

3.2. Effect of relative roughness pitch (P/e)

Figure 15 shows the plots of Nusselt number as a function of relative roughness pitch (*P/e*) for different values of Reynolds number and for fixed values of (a) *e/D* = 0.021, (b) *e/D* = 0.03 and (c) *e/D* = 0.042 for right-angle triangle rib roughness. For all types of ribs, it has been found that the Nusselt number decreases with an increase of relative roughness pitch and increases with increasing values of the Reynolds number in all investigated cases. This is due to the fact that with the increase in relative roughness pitch, the number of reattachment points over the absorber plate reduces. The roughened duct for all the three ribs with relative roughness pitch of 7.14 provides the highest Nusselt number at all range of Reynolds numbers. The minimum value of Nusselt number occurs at relative roughness pitch (*P/e*) of 35.71 for the range of parameters investigated for all three types of ribs used in this research work. It is also observed that for a given relative roughness height, the friction factor decreases with an increase of relative roughness pitch and decreases with increasing values of Reynolds number for all the three types of ribs roughness used in present analysis.

3.3. Effect of relative roughness height (e/D)

Figures 16 and 17 show the effect of relative roughness height (*e/D*) on the heat transfer performance for chamfered, right-angle triangular and reverse L-shaped rib. Figure 16 shows the plots of Nusselt number as a function of relative roughness height (*e/D*) for different values of Reynolds number and fixed value of relative roughness pitch, *P/e* = 7.14. The graphs shows that for a given

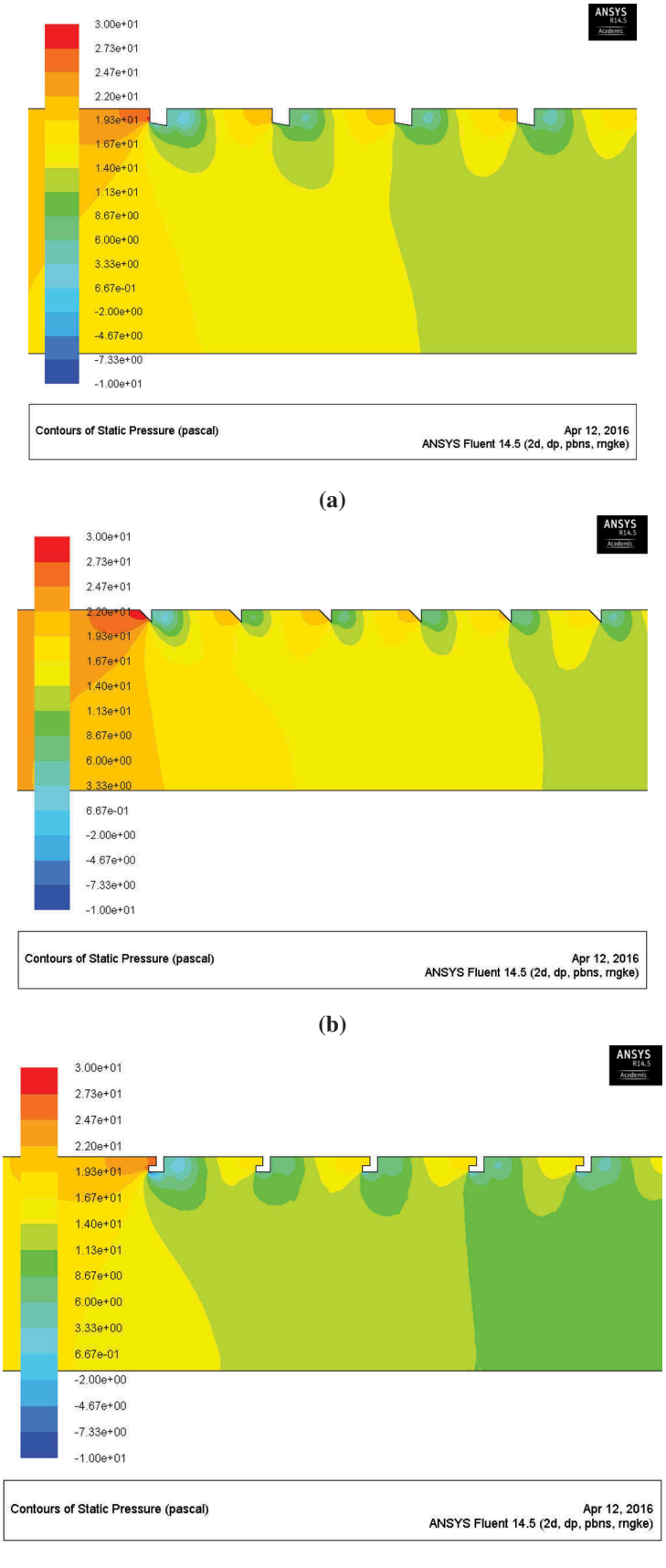

Figure 13. The contour plot of pressure for $P/e = 7.14$ and $e/D = 0.042$ at a Reynolds number of 15,000 for (a) 20° chamfered, (b) right-angle triangular and (c) reverse L-shaped rib roughness. (Gawande et al. 2016a, 2016b, 2016c).

relative roughness pitch the Nusselt number increases with an increase of relative roughness height and increases with increasing values of the Reynolds number and has been found maximum corresponding to relative roughness height of 0.042. This is due to the fact that heat transfer coefficient is low at the leading edge of all three

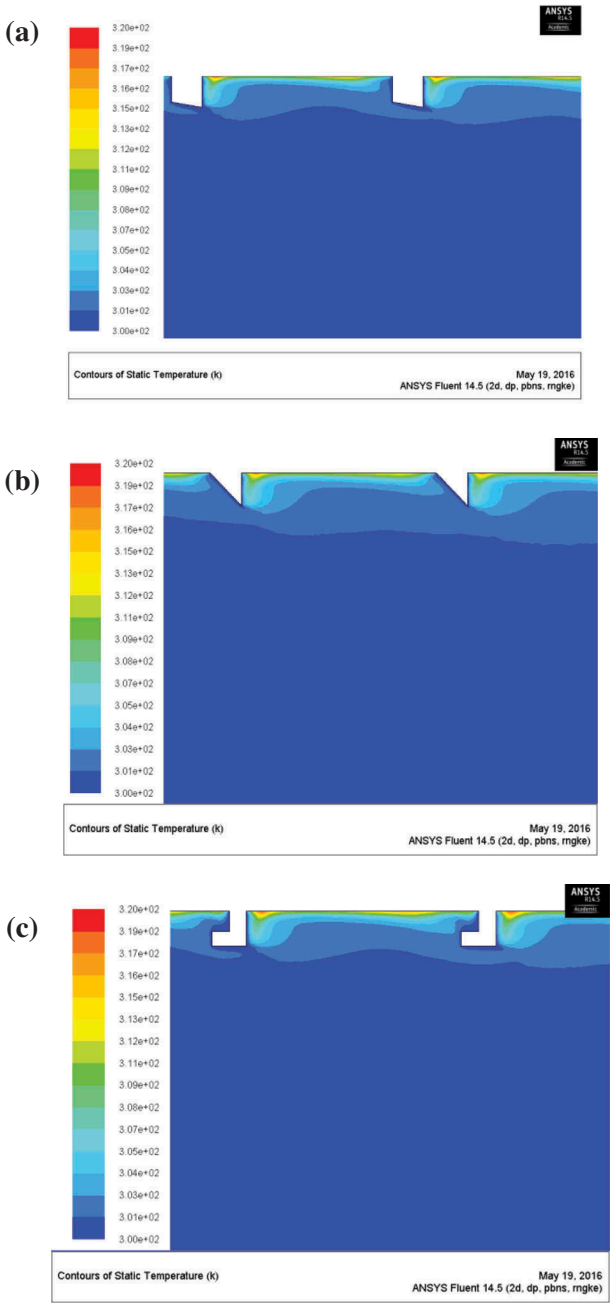

Figure 14. The contour plot of static temperature for *P/e* = 7.14 and *e/D* = 0.042 at a Reynolds number of 15,000 for (a) 20° chamfered, (b) right-angle triangular and (c) reverse L-shaped rib roughness. (Gawande et al. 2016a, 2016b, 2016c).

types of ribs and high at the trailing edge. Higher relative roughness height produced more reattachment of free shear layer, which creates the strong secondary flow. Hence, the heat transfer increases with increase in relative roughness height and maximum occurs at e/D of 0.042.

Figure 17 shows the plot of friction factor as a function of relative roughness height (*e/D*) for different values of Reynolds number and fixed *P/e* = 7.14. It is seen that for a given relative roughness pitch, the friction factor increases with an increase of relative roughness height and decreases with increasing values of the Reynolds number due to suppression of laminar sub-layer for fully developed flow in the duct, in all cases investigated in this work. It is also seen that the friction factor increases with increase in relative roughness height and has been found maximum corresponding to relative roughness height of 0.042.

3.4. Thermo-hydraulic performance parameter (T.H.P.P)

It has been observed that the rate of increment of average heat transfer is comparatively less than the rate of increment of average friction factor for increasing rib height. So, there is a need to choose the roughness geometry, which gives maximum heat transfer whilst keeping pumping losses to its least value. To achieve this, S.A.H. duct is analysed by simultaneous consideration of thermal and hydraulic performance. The thermo-hydraulic performance parameter based on constant pumping power requirement has been adopted for the optimisation of roughness and flow parameters for artificially roughened S.A.H.

The present experimental and C.F.D. investigations using three shapes of ribs on the absorber plate shows that the artificially roughened S.A.H. with relative roughness pitch of 7.14 and relative roughness height of 0.042 provide maximum value of average Nusselt number at a higher value of Reynolds number, *Re* = 15,000. Same artificially roughened S.A.H., with similar relative roughness pitch and relative roughness height, results in the maximum value of friction factor at lower value Reynolds number *Re* = 3800. It is, therefore, necessary to determine optimal rib dimension and arrangement such that the heat transfer coefficient is maximised whilst keeping the friction losses at the minimum possible value. A parameter that facilitates simultaneous consideration of thermal and hydraulic performance as defined by Webb and Eckert (1972) and is known as thermo-hydraulic performance parameter (T.H.P.P). The result of this parameter higher than unity declares the usefulness of applying an enhancement scheme and used to compare the performance of number of arrangements to decide the best amongst these. Thermo-hydraulic performance parameter comparison for square, chamfered, right-angle triangular and reverse L-shaped rib is shown in Figure 18. At relative roughness pitch (*P/e*) of 7.14, Reynolds number of 15,000 and relative roughness height (*e/D*) of 0.042, thermo-hydraulic performance parameter for square rib varies between 1.548 and 1.873. For chamfered square rib it varies between 1.577 and 2.047, between 1.41 and 2.035 for right-angle triangular rib and between 1.62 and 1.902 for reverse L-shaped rib roughness.

3.5. Validation of C.F.D. model

The experimentally investigated, average Nusselt number and friction factor of a S.A.H. with chamfered, right-

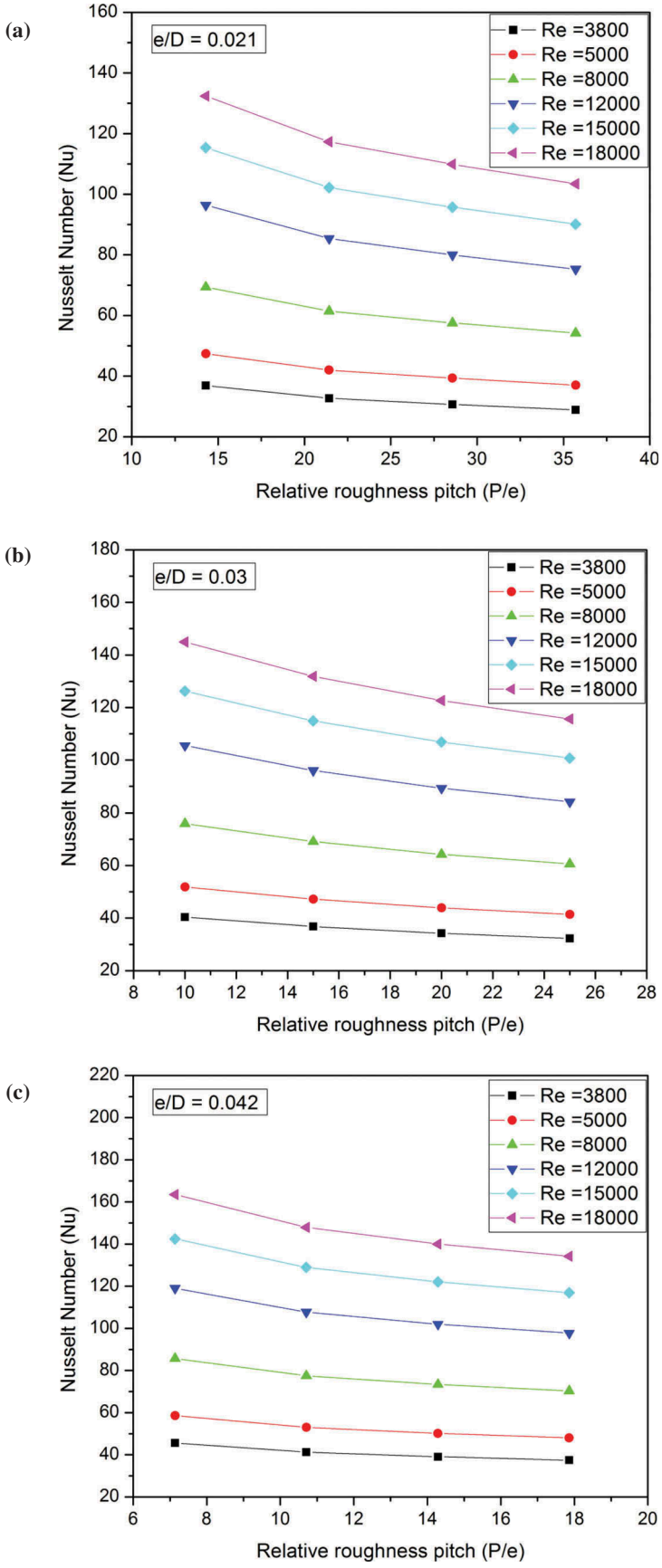

Figure 15. Nusselt number as a function of relative roughness pitch (*P/e*) for different values of Reynolds number and for (a) fixed *e/D* = 0.021, (b) fixed *e/D* = 0.03 (c) fixed *e/D* = 0.042, for right-angle triangular rib. (Gawande et al. 2016b).

angle triangular and reverse L-shaped rib roughness mounted on absorber plate is validated with the C.F.D. results under similar experimental operating conditions and for reverse L-shaped rib, it is shown in Figure 19. It has been found that the numerical results are in good agreement with the experimental results and are slightly under-predicted. The discrepancies for the Nusselt and friction factor values between the numerical results using

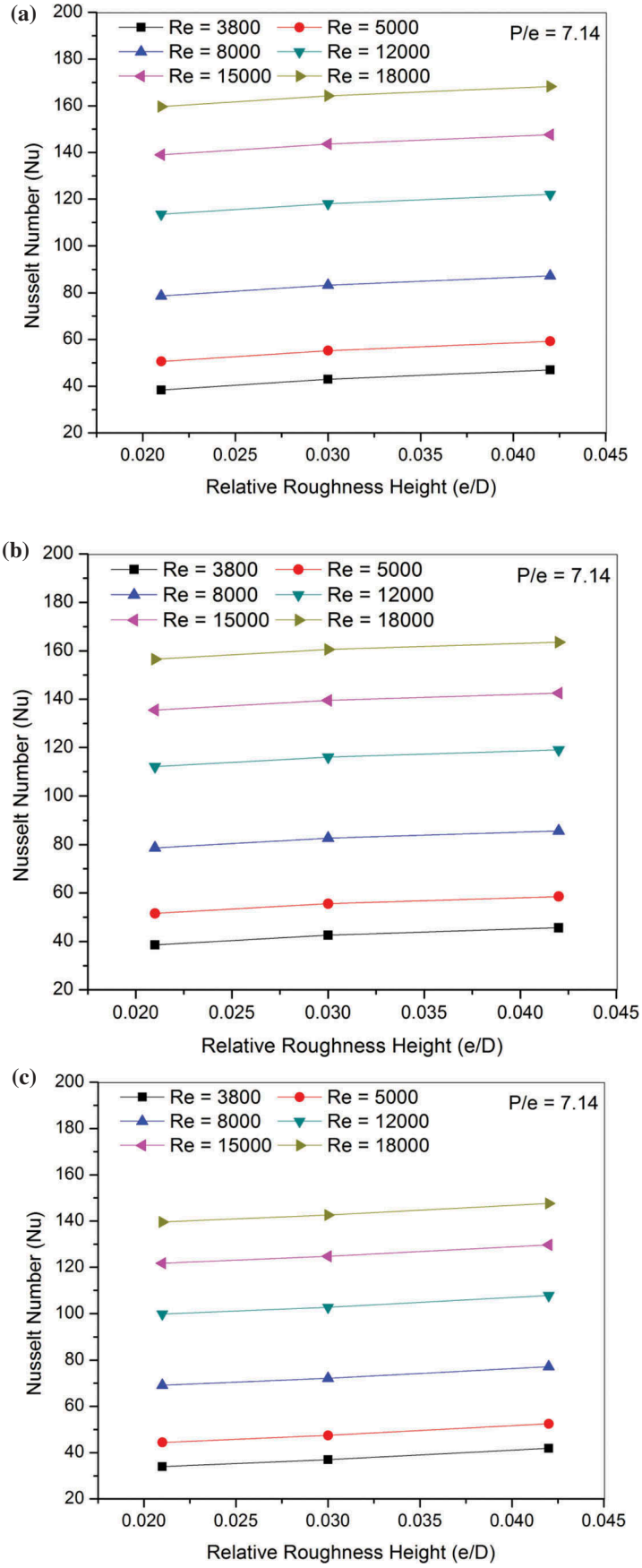

Figure 16. Nusselt number as a function of relative roughness height *e/D* for different values of Reynolds number and for fixed value of *P/e* for (a) chamfered rib, (b) right-angle triangular rib and (c) reverse L-shaped rib. Gawande et al. (2016a, 2016b, 2016c).

RNG k-ε turbulence model and the experimental results are less than ± 15%.

A literature search in this field revealed that within a certain limiting values of relative roughness pitch,

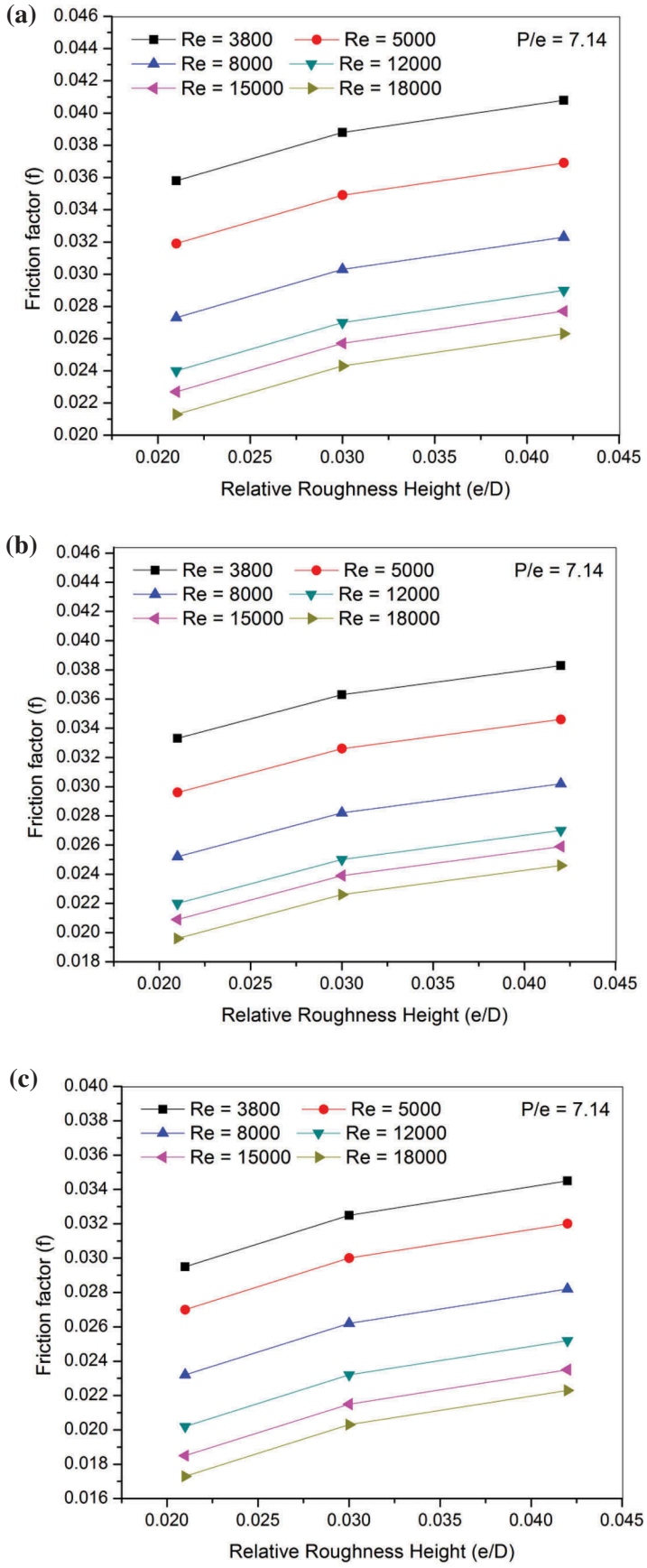

Figure 17. Friction factor as a function of relative roughness height *e/D* for different values of Reynolds number and for fixed value of *P/e* for (a) chamfered rib, (b) right-angle triangular rib and (c) reverse L-shaped rib. Gawande et al. (2016a, 2016b, 2016c).

artificially roughened S.A.H. performs thermo-hydraulically better than that of a smooth solar heater. This limiting value of relative roughness pitch has been found to lies in the range of 6–10. The C.F.D. and experimental results for all three types of ribs, shows that maximum heat transfer enhancement is observed for *P/e* = 7.14, which falls in between the accepted range of 6–10. Further, according to literature search in this

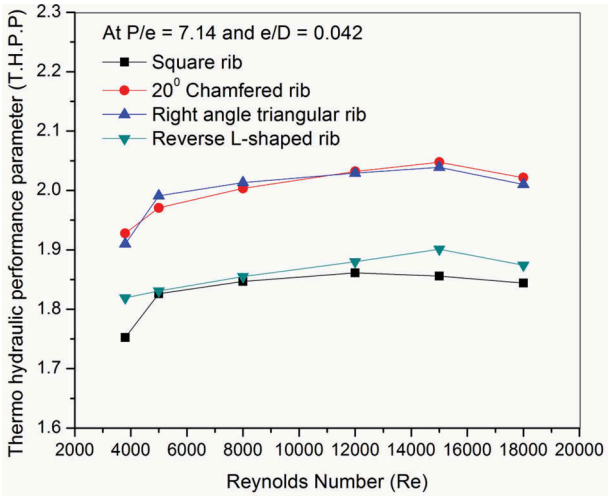

Figure 18. Comparison of thermo-hydraulic performance parameter (T.H.P.P) with Reynolds number for different values of relative roughness pitch for fixed *e/D* = 0.042 for various shapes of ribs. Gawande et al. (2016a, 2016b; 2016c).

area, the optimum value of relative roughness height generally lies in the range of 0.030–0.047 for better thermo-hydraulic performance. The value for the present experimental and C.F.D. analysis is also considered as 0.042, which in the accepted range for relative roughness height. Tables 4 and 5 show comparison of value of relative roughness pitch (*P/e*) and relative roughness height (*e/D*) for maximum heat transfer enhancement investigated experimentally and numerically by researchers, respectively.

3.6. Correlations

Statistical correlations are developed for Nusselt number and friction factor as a function of flow and geometrical parameters based on the experimental results for 20° chamfered, right-angle triangular and reverse L-shaped rib, presented in the following section. The correlations are useful for the prediction of thermo-hydraulic performance or to determine the optimum geometric parameters of roughness geometry for a particular application. The Nusselt number and friction factor correlations derived for chamfered, right-angle triangular and reverse L-shaped (Gawande et al. 2016a, 2016b, 2016c) ribs are follows:

3.7. Mathematical model (MATLAB code)

In this section, thermal and thermo-hydraulic performance of smooth as well as roughened S.A.H. has been investigated with the help of a mathematical model by generating a **MATLAB** code. Thermal and effective efficiency have been used as criteria for evaluating thermal and thermo-hydraulic performance of roughened S.A.H. The comparison graph in terms of thermal and effective efficiency for 20° chamfered, right-angle triangular and reverse L-shaped rib is plotted in Figure 20 with relative roughness height (*e/D*) of 0.04 and relative roughness pitch (*P/e*) of 7.14. The figure shows that thermal and effective efficiency tends to increase with the increase in Reynolds number for some interval and then again decreases for higher Reynolds number. This happens due to the dominance of the mechanical power, which is required to overcome the frictional forces in the duct. It is observed that the effective efficiency corresponding to the higher values of roughness height is better in the lower range of Reynolds number; however, the value of effective efficiency is reversed in the higher range of Reynolds number. This happens due to fact that at lower Reynolds number, the increase in the friction losses in the duct is insignificant with increase in relative roughness height, whilst the increase in heat transfer from roughened surface is quite substantial due to increase

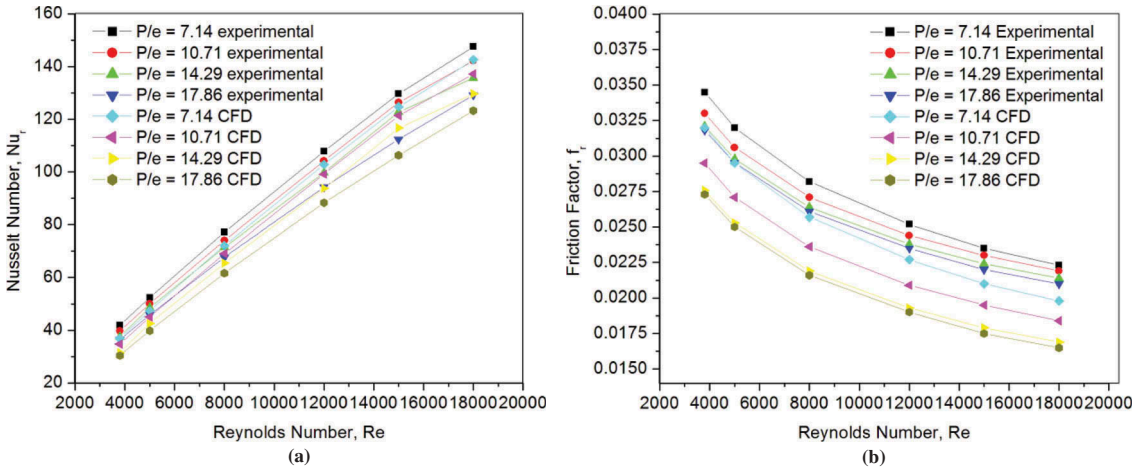

Figure 19. Comparison of experimentally and numerically (C.F.D.) calculated average (a) Nusselt number and (b) friction factor for reverse L-shaped rib. (Gawande et al. 2016c).

Table 4. Comparison of value of relative roughness pitch for maximum heat transfer enhancement investigated experimentally and numerically by researchers.

Sl. No.	Name of Author	Roughness geometry	Value of Relative Roughness Pitch, *P/e*
1	Prasad and Saini (1991)	Transverse wire rib roughness	*P/e* = 10
2	Aharwal, Gandhi and Saini (2008)	Inclined continuous rib roughness with gap	*P/e* = 10
3	Prasad and Mullick (1983)	Transverse wire rib roughness	*P/e* = 12.7
4	Varun, Saini, and Singal (2008)	Combination of transverse and inclined rib roughness	*P/e* = 8
5	Momin, Saini, and Solanki (2002)	V-shaped rib roughness	*P/e* = 10
6	Bhagoria, Saini, and Solanki (2002)	Transverse wedge-shaped rib roughness	*P/e* = 7.57
7	Jaurkar, Saini and Gandhi (2006)	Rib-grooved roughness	*P/e* = 6
8	Layek Saini and Solanki (2007)	Chamfered rib-grooved roughness	*P/e* = 6
9	Saini and Saini (1997)	Arc-shaped rib roughness	*P/e* = 10
10	Lanjewar, Bhagoria, and Sarviya (2011)	60° W-shaped rib roughness	*P/e* = 10
11	Bopche and Tandale (2009)	Inverted U-shaped rib roughness	*P/e* = 6.67
12	Yadav and Bhagoria (2014b)	Semicircular transverse ribs	*P/e* = 14.29
13	Yadav and Bhagoria (2013a)	Circular transverse rib	*P/e* = 10.71
14	Yadav and Bhagoria (2013b)	Square transverse rib	*P/e* = 10.71
15	Yadav and Bhagoria (2014a)	Equilateral triangular rib	*P/e* = 7.14
16	Sethi, Varun, and Thakur (2012)	Dimple-shaped elements	*P/e* = 10
17	Present experimental and numerical study (Gawande et al. 2016a,2016b,2016c]	Chamfered rib, Right-angle triangular rib and reverse L-shaped rib roughness	*P/e* = 7.14

Table 5. Comparison of value of relative roughness height for maximum heat transfer enhancement investigated experimentally and numerically by researchers.

S. No	Name of Author	Roughness geometry	Value of Relative Roughness height, *e/D*
1	Prasad and Saini (1991)	Transverse wire rib roughness	*e/D* = 0.033
2	Aharwal, Gandhi and Saini (2008)	Inclined continuous rib roughness with gap	*e/D* = 0.037
3	Varun, Saini, and Singal (2008)	Combination of transverse and inclined rib roughness	*e/D* = 0.030
4	Momin, Saini, and Solanki (2002)	V-shaped rib roughness	*e/D* = 0.032
5	Bhagoria, Saini, and Solanki (2002)	Transverse wedge-shaped rib roughness	*e/D* = 0.033
6	Jaurker, Saini, and Gandhi (2006)	Rib-grooved roughness	*e/D* = 0.0363
7	Layek, Saini, and Solanki (2007)	Chamfered rib-grooved roughness	*e/D* = 0.04
8	Saini and Saini (1997)	Arc-shaped rib roughness	*e/D* = 0.0422
9	Lanjewar, Bhagoria, and Sarviya (2011)	60° W-shaped rib roughness	*e/D* = 0.03375
10	Bopche and Tandale (2009)	Inverted U-shaped rib roughness	*e/D* = 0.0398
11	Yadav and Bhagoria (2014b)	Semicircular transverse ribs	*e/D* = **0**.042
13	Yadav and Bhagoria (2013a)	Circular transverse rib	*e/D* = 0.042
14	Yadav and Bhagoria (2013b)	Square transverse rib	*e/D* = 0.042
15	Yadav and Bhagoria (2014a)	Equilateral triangular rib	*e/D* = 0.042
16	Sethi, Varun, and Thakur (2012)	Dimple-shaped elements	*e/D* = 0.036
17	Present experimental and numerical study (Gawande, Dhoble and Gawande et al. 2016a, 2016b, 2016c)	Chamfered rib, Right-angle triangular rib and reverse L-shaped rib roughness	*e/D* = 0.042

For 20° chamfered rib, $Nu = 0.0943\ Re^{\circ.8248}\ (P/e)^{-0.3022}$

For right-angle triangular rib, $Nu = 133.36*Re^{\circ.8183}*(e/D)^{3.6305}*(\exp 0.4480*\ln(e/D)^2)*(P/e)^{-0.4807}$ *exp $(0.055*\ln(P/e)^2)$

For reverse L-shaped rib, $Nu = 0.032Re^{\circ.8332}\ (P/e)^{\ 0.3479}\ \exp\ (-0.1004\ln\ (P/e)^{\ 2})$

For 20° chamfered rib, $f = 0.653\ Re^{-0.2883}\ (P/e)^{-0.2087}$

For Right-angle triangular rib, $f = 42.979Re^{-0.2778}(e/D)^{1.1517}\exp(0.1105\ln(e/D)^2)(P/e)^{-1.7453}\exp(0.3133\ln(P/e)^2)$

For reverse L-shaped rib, $f = 0.2805\ Re^{-0.2617}(P/e)^{\circ.0815}\exp(-0.0319\ln(P/e)^2)$

of turbulence in the vicinity of roughened surface. For the range of system and operating parameters, maximum enhancement in thermal and effective efficiency for roughened S.A.H. has been found of the order of 1.6 and 2.2 times, respectively, as compared to S.A.H. having smooth absorber plate. In all cases, the percentage increase in thermal and effective efficiency is higher for 20° chamfered rib, followed by right-angle triangular and then reverse L-shaped rib (Gawande et al. 2016a, 2016b, 2016c).

4. Conclusions

An experimental and C.F.D. investigation has been carried out by mounting chamfered, right-angle triangular and reverse L-shaped rib roughness on a absorber plate to study the heat transfer performance and friction factor characteristics by optimising the dimensions of the air heater construction elements. In this work, the performance of S.A.H. is evaluated by predicting the effect of geometrical parameters such as rib height (e), pitch (P) and operating parameters such as relative roughness pitch (P/e), relative roughness height (e/D), duct aspect ratio (W/H) and

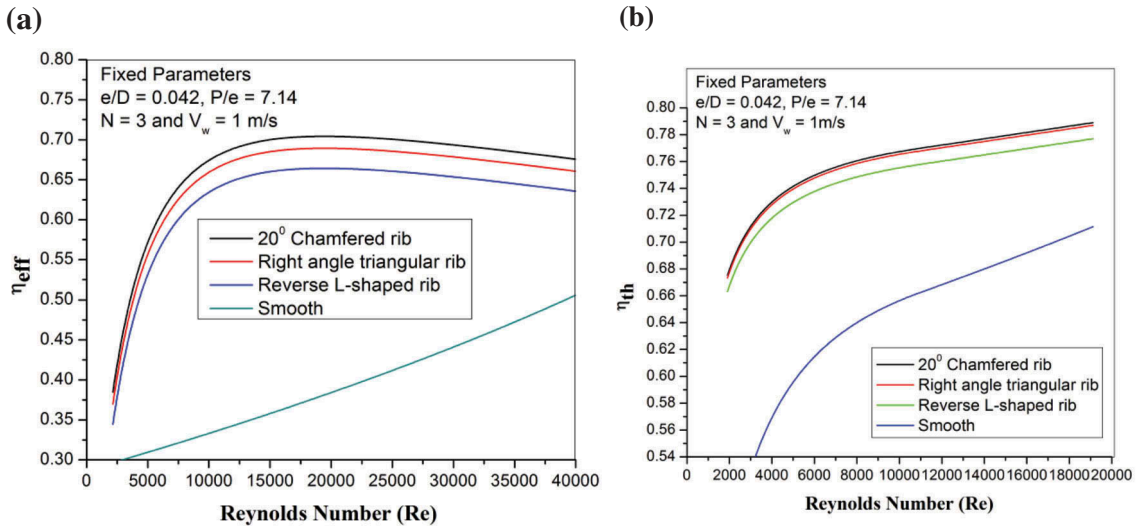

Figure 20. Comparison of (a) effective efficiency and (b) thermal efficiency vs. Reynolds number for roughened and smooth air heaters (Gawande et al. 2016e).

chamfer angle (α). The experimental data have also been used to develop statistical correlations for Nusselt number and friction factor for chamfered, right-angle triangular and reverse L-shaped rib roughened S.A.H. An analytical model has been developed based upon which the thermal efficiency and effective efficiency has been evaluated for optimised roughness parameters of all ribs for specified operating condition of S.A.H. The following are the key outcomes from the present work:

(1) The experimental and C.F.D. analysis of chamfered square rib with chamfer angle varying from α = 0° – 40° is conducted. The chamfered square rib with 20° chamfer angle is found to provide best thermo-hydraulic performance and, hence, selected for further thermal analysis.
(2) Very few investigations have been conducted in S.A.H. at relative roughness pitch (*P/e*) less than the suggested optimum value in the literature. Literature review reveals that maximum heat transfer enhancement is predicted at optimum configuration of relative roughness pitch, in the range of 8–10. But with this kind of turbulators, Nusselt number increases continuously with reducing pitch ratio values.
(3) Maximum enhancement in Nusselt number for 20° chamfered, right-angle triangular and reverse L-shaped rib roughness is found to be 3.218, 3.10 and 2.827 times over smooth duct for relative roughness pitch (*P/e*) of 7.14, Reynolds number (*Re*) of 15,000 at relative roughness height (*e/D*) of 0.042.
(4) Maximum enhancement in average friction factor for 20° chamfered, right-angle triangular and reverse L-shaped rib roughness is found to be 4.047, 3.80 and 3.424 times over smooth duct for relative roughness pitch (*P/e*) of 7.14, Reynolds number (*Re*) of 3800 at relative roughness height (*e/D*) of 0.042.
(5) Thermo-hydraulic performance parameter (T.H.P.P) is evaluated for all the three rib designs to determine the optimal rib dimension and arrangement that will result in maximum enhancement in heat transfer with minimum friction penalty. At relative roughness pitch (*P/e*) of 7.14, Reynolds number of 15,000 and relative roughness height (*e/D*) of 0.042, thermo-

Table 6. Comparison of thermo-hydraulic performance parameter of present investigation with previous literature results.

Sl. No.	References	Roughness geometry	Duct aspect ratio (W/H)	Relative roughness pitch (P/e)	T.H.P.P
1	Bhagoria, Saini, and Solanki (2002)	Transverse wedge-shaped rib roughness	5	7.57	**1.95**
2	Jaurker, Saini, and Gandhi (2006)	Rib grooved roughness	7	6	**1.82**
3	Layek, Saini, and Solanki (2007)	Chamfered rib and groove roughness	5	5	**1.74**
4	Yadav and Bhagoria (2014a)	Equilateral triangle sectioned ribs	5	7.14	**2.11**
5	**Present study** (Gawande et al. 2016a, 2016b, 2016c).	1) 20 chamfered rib 2) Right-angle triangular rib 3) Reverse L-shaped rib	5	7.14	**1) 2.047** **2) 2.035** **3) 1.903**

hydraulic performance parameter for 20° chamfered rib, right-angle triangular rib and reverse L-shaped rib varies between 1.577 and 2.047, between 1.41 and 2.03 and between 1.62 and 1.90 respectively. The experimental and numerical results obtained in the present work are compared with the previous literature results under and are shown in Table 6.

(6) The experimental data corresponding to 20° chamfered, right-angle triangular and reverse L-shaped rib roughened duct are used for regression analysis to develop statistical relationships that yield best fit equations for Nusselt number and friction factor as a function of geometrical and flow parameters.

(7) Based upon the correlations developed, the thermal and thermo-hydraulic performance of 20° chamfered, right-angle triangular and reverse L-shaped rib roughened S.A.H. has been carried out analytically using MATLAB code. For the range of system and operating parameters, maximum enhancement in thermal and effective efficiency for roughened S.A.H. has been found of the order of 1.6 and 2.2 times, respectively, as compared to S.A.H. having smooth absorber plate. In all cases, the percentage increase in thermal and effective efficiency is higher for 20° chamfered rib, followed by right-angle triangular and then reverse L-shaped rib.

Disclosure statement

No potential conflict of interest was reported by the authors.

Notes on contributors

Dr. Vipin B. Gawande is currently working as an Assistant Professor in the Department of Mechanical Engineering at Vidya Pratishthan's Kamal Nayan Bajaj Institute of Engineering and Technology, Baramati, India. His research interest includes Solar energy, Heat Transfer, CFD etc.

DA. S. Dhoble is currently working as an Assistant Professor in the Department of Mechanical Engineering at Visvesvaraya National Institute of Technology, Nagpur-India. His research interest includes Automobile Engineering, Solar and Thermal Engineering etc.

D. B. Zodpe is currently working as an Associate Professor in the Department of Mechanical Engineering at Visvesvaraya National Institute of Technology, Nagpur-India. His research interest includes Refrigeration and Air Conditioning, HVAC, Automobile and Thermal Engineering.

Chidanand Mangrulkar is a research scholar in the Department of Mechanical Engineering at Visvesvaraya National Institute of Technology, Nagpur-India.

ORCID

Vipin B. Gawande http://orcid.org/0000-0002-2440-9156

References

Aharwal, K. R., B. K. Gandhi, and J. S. Saini. 2008. "Experimental Investigation on Heat-Transfer Enhancement Due to a Gap in an Inclined Continuous Rib Arrangement in a Rectangular Duct of Solar Air Heater." *Renewable Energy* 33 (4): 585–596. doi:10.1016/j.renene.2007.03.023.

Ammari, H. D. 2003. "A Mathematical Model of Thermal Performance of A Solar Air Heater with Slats." *Renewable Energy* 28 (10): 597–1615. doi:10.1016/S0960-1481(02)00253-7.

ASHRAE Standard 93-77. 1977. *Method of Testing to Determine the Thermal Performance of Solar Air Heater*. New York, pp. 1e34. https://ashrae.iwrapper.com/ViewOnLine/Standard_93-1977

Bhagoria, J. L., J. S. Saini, and S. C. Solanki. 2002. "Heat Transfer Coefficient and Friction Factor Correlations for Rectangular Solar Air Heater Duct Having Transverse Wedge Shaped Rib Roughness on the Absorber Plate." *Renewable Energy* 25 (3): 341–369. doi:10.1016/S0960-1481(01)00057-X.

Bhushan, B., and R. Singh. 2012. "Thermal and Thermo Hydraulic Performance of Roughened Solar Air Heater Having Protruded Absorber Plate." *Solar Energy* 86 (11): 3388–3396. doi:10.1016/j.solener.2012.09.004.

Bopche, S. B., and M. S. Tandale. 2009. "Experimental Investigation on Heat Transfer and Frictional Characteristics of a Turbulator Roughened Solar Air Heater Duct." *International Journal of Heat and Mass Transfer* 52 (11–12): 2834–2848. doi:10.1016/j.ijheatmasstransfer.2008.09.039.

Fox, W., Pritchard, and A. McDonald. 2010. *Introduction to Fluid Mechanics*. New York: John Wiley & Sons.

Gawande, V. B., A. S. Dhoble, and D. B. Zodpe. 2014. "Effect of Roughness Geometries on Heat Transfer Enhancement in Solar Thermal systems–A Review." *Renewable and Sustainable Energy Reviews* 32: 347–378. doi:10.1016/j.rser.2014.01.024.

Gawande, V. B., A. S. Dhoble, D. B. Zodpe, and S. Chamoli. 2016a. "Experimental and CFD-based Thermal Performance Prediction of Solar Air Heater Provided with Chamfered Square Rib as Artificial Roughness." *Journal of the Brazilian Society of Mechanical Sciences and Engineering* 38 (2): 643–663. doi:10.1007/s40430-015-0402-9.

Gawande, V. B., A. S. Dhoble, D. B. Zodpe, and S. Chamoli. 2016b. "Experimental and CFD-based Thermal Performance Prediction of Solar Air Heater Provided with Right-Angle Triangular Rib as Artificial Roughness." *Journal of the Brazilian Society of Mechanical Sciences and Engineering* 38 (2): 551–579. doi:10.1007/s40430-015-0391-8.

Gawande, V. B., A. S. Dhoble, D. B. Zodpe, and S. Chamoli. 2016c. "Experimental and CFD Based Thermo Hydraulic Performance Evaluation of a Solar Air Heater with Reverse L-Shaped Rib Roughness on Absorber Plate." *Solar Energy* 131: 275–295. doi:10.1016/j.solener.2016.02.040.

Gawande, V. B., A. S. Dhoble, D. B. Zodpe, and S. Chamoli. 2016d. "A Review of CFD Methodology Used in

Literature for Predicting Thermo-Hydraulic Performance of A Roughened Solar Air Heater." *Renewable and Sustainable Energy Reviews* 54: 550–605. doi:10.1016/j.rser.2015.10.025.

Gawande, V. B., A. S. Dhoble, D. B. Zodpe, and S. Chamoli. 2016e. "Analytical Approach for Evaluation of Thermal Hydraulic Performance of Roughened Solar Air Heater." *Case Studies in Thermal Engineering* 8: 19–31. doi:10.1016/j.csite.2016.03.003.

Gupta, A. D., and L. Varshney. 2017. "Performance Prediction for Solar Air Heater Having Rectangular Sectioned Tapered Rib Roughness Using CFD." *Thermal Science and Engineering Progress* 4: 122–132. doi:10.1016/j.tsep.2017.09.005.

Jaurker, A. R., J. S. Saini, and B. K. Gandhi. 2006. "Heat Transfer and Friction Characteristics of Rectangular Solar Air Heater Duct Using Rib-Grooved Artificial Roughness." *Solar Energy* 80 (8): 895–907. doi:10.1016/j.solener.2005.08.006.

Kumar, R., and A. Kumar. 2017. "A Parametric Study of the 2D Model of Solar Air Heater with Elliptical Rib Roughness Using CFD." *Journal of Mechanical Science and Technology* 31 (2): 959–964. doi:10.1007/s12206-017-0253-7.

Kumar, R., V. Goel, and A. Kumar. 2018. "Investigation of Heat Transfer Augmentation and Friction Factor in Triangular Duct Solar Air Heater Due to Forward Facing Chamfered Rectangular Ribs: A CFD Based Analysis." *Renewable Energy* 115: 824–835. doi:10.1016/j.renene.2017.09.010.

Kumar, R., V. Goel, A. Kumar, S. Khurana, P. Singh, and S. B. Bopche. 2018. "Numerical Investigation of Heat Transfer and Friction Factor in Ribbed Triangular Duct Solar Air Heater Using Computational Fluid Dynamics (C.F.D.)." *Journal of Mechanical Science and Technology* 32 (1): 399–404. doi:10.1007/s12206-017-1240-8.

Lanjewar, A., J. L. Bhagoria, and R. M. Sarviya. 2011. "Experimental Study of Augmented Heat Transfer and Friction in Solar Air Heater with Different Orientations of W-Rib Roughness." *Experimental Thermal and Fluid Science* 35 (6): 986–995. doi:10.1016/j.expthermflusci.2011.01.019.

Layek, A., J. S. Saini, and S. C. Solanki. 2007. "Second Law Optimization of a Solar Air Heater Having Chamfered Rib-Groove Roughness on Absorber Plate." *Renewable Energy* 32 (12): 1967–1980. doi:10.1016/j.renene.2006.11.005.

McAdams, W. H. 1942. *Heat Transmission*. New York: Mc Graw-Hill.

Momin, A. M. E., J. S. Saini, and S. C. Solanki. 2002. "Heat Transfer and Friction in Solar Air Heater Duct with V-Shaped Rib Roughness on Absorber Plate." *International Journal of Heat and Mass Transfer* 45 (16): 3383–3396. doi:10.1016/S0017-9310(02)00046-7.

Ong, K. S. 1995. "Thermal Performance of Solar Air Heaters: Mathematical Model and Solution Procedure." *Solar Energy* 55 (2): 93–109. doi:10.1016/0038-092X(95)00021-I.

Patankar, S. V. 1980. *Numerical Heat Transfer and Fluid Flow*. Washington DC: Hemisphere.

Prasad, B. N., and J. S. Saini. 1991. "Optimal Thermo Hydraulic Performance of Artificially Roughened Solar Air Heaters." *Solar Energy* 47 (2): 91–96. doi:10.1016/0038-092X(91)90039-Y.

Prasad, K., and S. C. Mullick. 1983. "Heat Transfer Characteristics of a Solar Air Heater Used for Drying Purposes." *Applied Energy* 13 (2): 83–93.. doi:10.1016/0306-2619(83)90001-6.

Ravi, R. K., and R. P. Saini. 2018. "Effect of Roughness Elements on Thermal and Thermohydraulic Performance of Double Pass Solar Air Heater Duct Having Discrete Multi V-Shaped and Staggered Rib Roughness on Both Sides of the Absorber Plate." *Experimental Heat Transfer* 31 (1): 47–67. doi:10.1080/08916152.2017.1350217.

Saini, R. P., and J. S. Saini. 1997. "Heat Transfer and Friction Factor Correlations for Artificially Roughened Ducts with Expanded Metal Mesh as Roughened Element." *International Journal of Heat and Mass Transfer* 40 (4): 973–986. doi:10.1016/0017-9310(96)00019-1.

Sethi, M., G. Varun, and N. S. Thakur. 2012. "Correlations for Solar Air Heater Duct with Dimpled Shape Roughness Elements on Absorber Plate." *Solar Energy* 86 (9): 2852–2861. doi:10.1016/j.solener.2012.06.024.

Shamardan, M. M., M. Norouzi, M. H. Kayhani, and A. A. Delouei. 2012. "An Exact Analytical Solution for Convective Heat Transfer in Rectangular Ducts." *Journal of Zhejiang University SCIENCE A* 13 (10): 768–781. https://link.springer.com/article/10.1631/jzus.A1100122.

Singh, I., and S. Singh. 2018. "CFD Analysis of Solar Air Heater Duct Having Square Wave Profiled Transverse Ribs as Roughness Elements." *Solar Energy* 162: 442–453. doi:10.1016/j.solener.2018.01.019.

Varun, R. P. Saini, and S. K. Singal. 2008. "Investigation of Thermal Performance of Solar Air Heater Having Roughness Elements as a Combination of Inclined and Transverse Ribs on the Absorber Plate." *Renewable Energy* 33 (6): 1398–1405. doi:10.1016/j.renene.2007.07.013.

Webb, R. L., and E. R. G. Eckert. 1972. "Application of Rough Surface to Heat Exchanger Design." *International Journal Heat and Mass Transfer* 15 (9): 1647–1658. doi:10.1016/0017-9310(72)90095-6.

Yadav, A. S., and J. L. Bhagoria. 2013a. "A CFD (Computational Fluid Dynamics) Based Heat Transfer and Fluid Flow Analysis of A Solar Air Heater Provided with Circular Transverse Wire Rib Roughness on the Absorber Plate." *Energy* 55: 1127–1142.. doi:10.1016/j.energy.2013.03.066.

Yadav, A. S., and J. L. Bhagoria. 2013b. "Modeling and Simulation of Turbulent Flows through a Solar Air Heater Having Square-Sectioned Transverse Rib Roughness on the Absorber Plate." *Hindawi Publishing Corporation. The Scientific World Journal* 2013: 12. Article ID 827131. doi:10.1155/2013/827131.

Yadav, A. S., and J. L. Bhagoria. 2014a. "A CFD Based Thermo-Hydraulic Performance Analysis of an Artificially Roughened Solar Air Heater Having Equilateral Triangular Sectioned Rib Roughness on the Absorber Plate." *International Journal of Heat and Mass Transfer* 70: 1016–1039. doi:10.1016/j.ijheatmasstransfer.2013.11.074.

Yadav, A. S., and J. L. Bhagoria. 2014b. "A Numerical Investigation of Turbulent Flows Through an Artificially Roughened Solar Air Heater." *Numerical Heat Transfer, Part A: Applications* 65 (7): 679–698. doi:10.1080/10407782.2013.846187.